

# Enhancing quantum vacuum signatures with tailored laser beams

Felix Karbstein<sup>1,2,\*</sup> and Elena A. Mosman<sup>3,†</sup>

<sup>1</sup>*Helmholtz-Institut Jena, Fröbelstieg 3, 07743 Jena, Germany*

<sup>2</sup>*Theoretisch-Physikalisches Institut, Abbe Center of Photonics,*

*Friedrich-Schiller-Universität Jena, Max-Wien-Platz 1, 07743 Jena, Germany*

<sup>3</sup>*National Research Tomsk Polytechnic University, Lenin Ave. 30, 634050 Tomsk, Russia*

(Dated: April 10, 2020)

We demonstrate that tailored laser beams provide a powerful means to make quantum vacuum signatures in strong electromagnetic fields accessible in experiment. Typical scenarios aiming at the detection of quantum vacuum nonlinearities at the high-intensity frontier envision the collision of focused laser pulses. The effective interaction of the driving fields mediated by vacuum fluctuations gives rise to signal photons encoding the signature of quantum vacuum nonlinearity. Isolating a small number of signal photons from the large background of the driving laser photons poses a major experimental challenge. The main idea of the present work is to modify the far-field properties of a driving laser beam to exhibit a field-free hole in its center, thereby allowing for an essentially background free measurement of the signal scattered in the forward direction. Our explicit construction makes use of a peculiar far-field/focus duality.

*Introduction* Maxwell’s classical theory of electrodynamics provides an accurate theoretical description of the physics of macroscopic electromagnetic fields. One of its cornerstones is the superposition principle, implying that light rays pass through each other without interaction and do not change their properties. However, as a purely classical theory, Maxwell’s electrodynamics should arise from the more fundamental theory of quantum electrodynamics (QED) in the formal limit of  $\hbar \rightarrow 0$ . The true theory of vacuum electrodynamics differs from Maxwell theory by terms suppressed parametrically with  $\hbar$ . The leading corrections were determined as early as in the 1930s by Heisenberg and Euler [1, 2], who studied the effective self-interactions of slowly varying electromagnetic fields induced by vacuum fluctuations of electrons and positrons. These non-linear couplings facilitate light-by-light scattering phenomena, which – at least in principle – invalidate the superposition principle. Having no tree-level analogue, they are suppressed with inverse powers of the electron mass  $m_e$ , making them very elusive in experiment; see the Reviews [3–11] and references therein.

The advent of high-intensity laser facilities [12–15] opens up the possibility of verifying QED vacuum nonlinearities in macroscopically controlled fields. All-optical signatures, i.e., effects driven by laser fields resulting in photonic signals, are the prime candidates for such discovery experiments. However, the large background of the driving laser photons typically constitutes a major obstacle in measuring the signal. In this letter, we demonstrate that tailored laser beams featuring a peak in the focus where the interaction takes place, but a hole in the far field where the signal is measured provide a novel means to overcome these limitations; we work in Heaviside-Lorentz units with  $c = \hbar = 1$ .

*Pulsed laser fields* For definiteness, we only consider a specific class of monochromatic laser fields of oscillation frequency  $\omega = \frac{2\pi}{\lambda}$ , which are rotationally symmetric

about the beam axis and are well-described by focused beam solutions of the paraxial wave equation. These are valid for small asymptotic beam divergences  $\theta \simeq \frac{w_0}{z_R}$ , with waist  $w_0$  and Rayleigh range  $z_R = \frac{\pi w_0^2}{\lambda}$  of the fundamental Gaussian (FG<sub>0</sub>) mode. By construction, they violate the wave equation at  $\mathcal{O}(\theta)$ . FG<sub>0</sub> beams focused to  $w_0 \gtrsim \lambda$  fulfill  $\theta \lesssim \frac{1}{\pi}$  rad. To describe laser pulses of finite duration  $\tau$ , we supplement these beam solutions with a Gaussian pulse envelope. This *ad hoc* prescription inevitably violates the wave equation at  $\mathcal{O}(\frac{1}{\tau\omega})$ . For typical high-intensity (free-electron) laser pulse parameters  $\tau \geq 20$  fs (2 fs) and  $\omega \geq 1.5$  eV (3 keV) we have  $\tau\omega \gtrsim 43.2$  (8700), rendering this approximation well-justified.

We focus on linearly polarized laser pulses which can be expressed as superposition of Laguerre-Gaussian LG<sub>*p,l*</sub> modes [16, 17] with  $l = 0$ , but finite  $p \in \mathbb{N}_0$ . The field profile associated with the LG<sub>*p,0*</sub> mode is denoted by  $\mathcal{E}_p$ . Hence, for a pulse propagating in  $\hat{\kappa}$  direction we have  $\vec{E}(x) = E(x)\hat{e}_E$ ,  $\vec{B}(x) = E(x)\hat{e}_B$  and  $E(x) = \sum_p \mathcal{E}_p(x)$ ; the unit vectors fulfill  $\hat{e}_E \cdot \hat{e}_B = 0$  and  $\hat{e}_E \times \hat{e}_B = \hat{\kappa}$ .

To allow for a compact representation of  $\mathcal{E}_p(x)$ , we identify the beam axis with the  $z$  axis and use cylindrical coordinates  $(r, \varphi, z)$ ; the focus is at  $z = 0$ . Here,  $z$  is the longitudinal coordinate along the beam axis,  $r$  is the radial distance and  $\varphi$  the azimuth. Moreover, we introduce the shorthand notations  $\zeta = \frac{z}{z_R}$  and  $\chi = \frac{r}{w(\zeta)}$ , where  $w(\zeta) = w_0 \sqrt{1 + \zeta^2}$  is the radius of the FG<sub>0</sub> mode. In these coordinates, we have [16, 17]

$$\mathcal{E}_p(x) = \mathfrak{E}_p e^{-\left(\frac{z-t}{\tau/2}\right)^2} \frac{w_0}{w(\zeta)} L_p(2\chi^2) e^{-\chi^2} \cos(\Phi_p(x)), \quad (1)$$

with Laguerre polynomials  $L_p(2\chi^2) = \sum_{j=0}^p \frac{(-2)^j}{j!} \binom{p}{j} \chi^{2j}$ . The peak field amplitude  $\mathfrak{E}_p$  is related to the mode energy  $W_p$  via  $\mathfrak{E}_p^2 \simeq 8 \sqrt{\frac{2}{\pi}} \frac{W_p}{\pi w_0^2 \tau}$  [18], and the phase  $\Phi_p(x)$  reads

$$\Phi_p(x) = \omega(z - t) + \zeta \chi^2 - (2p + 1) \arctan \zeta + \varphi_p. \quad (2)$$

The second term in Eq. (2) accounts for wavefront curvature effects, the third one is the mode's Gouy phase shift, and the last one is a mode-specific constant phase.

The laser intensity is defined as  $I = |\langle \vec{E} \times \vec{B} \rangle_t| = \langle E^2 \rangle_t = \sum_{p,p'} \langle \mathcal{E}_p \mathcal{E}_{p'} \rangle_t$ , where  $\langle \cdot \rangle_t$  denotes averaging over one laser period. To determine it we average over the oscillatory terms in  $\mathcal{E}_p \mathcal{E}_{p'} \sim \cos(\Phi_p(x)) \cos(\Phi_{p'}(x))$ . Up to subleading corrections of  $\mathcal{O}(\frac{1}{\tau\omega})$ , anyhow not consistently accounted for from the outset, the pulse envelope is not affected by the averaging procedure. This yields

$$I(x) = 4\sqrt{\frac{2}{\pi}} e^{-2(\frac{z-t}{\tau/2})^2} \frac{1}{1+\zeta^2} \sum_{p,p'} \frac{\sqrt{W_p W_{p'}}}{\pi w_0^2 \tau} \times \cos[2(p'-p) \arctan \zeta + \varphi_p - \varphi_{p'}] \times L_p(2\chi^2) L_{p'}(2\chi^2) e^{-2\chi^2}. \quad (3)$$

The pulse energy is  $W = 2\pi \int_0^\infty dr r \int_{-\infty}^\infty dt I(x) = \sum_p W_p$ .

In the far field  $\zeta \gg 1$ , we have  $\chi|_{\zeta \gg 1} \simeq \frac{r}{w_0 \zeta} = \frac{\vartheta}{\theta}$ , where  $\vartheta$  is the polar angle measured relative to the beam axis. Due to the exponential decay of the intensity (3) with  $e^{-2\chi^2}$  and the fact that  $\theta$  is small for paraxial beams by definition, the approximation  $\vartheta \simeq \frac{r}{z} \ll 1$  is well-justified here. Correspondingly, the pulse energy can be recast as  $W \simeq 2\pi(\frac{w_0}{\theta})^2 \int_0^\infty d\vartheta \vartheta \int_{-\infty}^\infty dt \zeta^2 I(\zeta \gg 1)$ . From this expression, we infer that the far-field angular decay of the number of laser photons  $N \simeq \frac{W}{\omega}$  with  $\vartheta$  is described by  $\frac{dN}{d\vartheta} \simeq \frac{2\pi}{\omega} (\frac{w_0}{\theta})^2 \int_{-\infty}^\infty dt \zeta^2 I(\zeta \gg 1)$ .

In the focus at  $\zeta = 0$  the cosine in Eq. (3) becomes  $\cos(\varphi_p - \varphi_{p'})$ , while in the far field at  $\zeta \gg 1$  it equals  $(-1)^{p'-p} \cos(\varphi_p - \varphi_{p'})$ . This implies that only for  $p' = p$ , i.e., laser fields prepared in a pure LG mode, the transverse intensity profiles in the focus and the far field have the same shape. For generic laser fields, terms with  $p' \neq p$  result in differently shaped focus and far-field profiles.

*Flattened-Gaussian field profiles* Following Refs. [18, 19], it can be straightforwardly shown that in order to implement the flattened-Gaussian (FG $_{\mathcal{N}}$ ) radial field profile

$$E_{\mathcal{N}}(\chi) \sim e^{-\chi^2} \sum_{n=0}^{\mathcal{N}} \frac{1}{n!} \chi^{2n}, \quad (4)$$

with  $\mathcal{N} \in \mathbb{N}_0$ , at a given value of the longitudinal coordinate  $z = z_0 \leftrightarrow \zeta_0 = \frac{z_0}{z_R}$ , the mode-specific phases and energies in Eqs. (1)-(3) have to be chosen as

$$\begin{aligned} \varphi_p &\rightarrow p(\pi + 2 \arctan \zeta_0), \\ W_p &\rightarrow \left( \frac{c_{p,\mathcal{N}}}{C_{\mathcal{N}}} \right)^2 W, \end{aligned} \quad (5)$$

and the sums over  $p, p'$  be restricted to all integers from 0 to  $\mathcal{N}$ . We denote the field and intensity profiles of the laser pulse featuring a FG $_{\mathcal{N}}$  field profile (4) at  $z = z_0$  by  $E_{\mathcal{N}}^{\zeta_0}(x)$  and  $I_{\mathcal{N}}^{\zeta_0}(x)$ . FG $_{\mathcal{N}}$  beams with  $\mathcal{N} \gg 1$  closely resemble super-Gaussian beams [20]. The coefficients in Eq. (5) are determined by the expansion coefficients of

the Exponential Sum Function in the Laguerre basis,  $\sum_{n=0}^{\mathcal{N}} \frac{1}{n!} \chi^{2n} = \sum_{p=0}^{\mathcal{N}} (-1)^p c_{p,\mathcal{N}} L_p(2\chi^2)$ , and read [18, 19]

$$c_{p,\mathcal{N}} = \sum_{k=p}^{\mathcal{N}} \binom{k}{p} \frac{1}{2^k}, \quad C_{\mathcal{N}}^2 = \sum_{p=0}^{\mathcal{N}} c_{p,\mathcal{N}}^2. \quad (6)$$

For  $\mathcal{N} = 0$  we recover the fundamental Gaussian beam. At  $z = z_0$ , where it features a FG $_{\mathcal{N}}$  profile and  $\chi = \frac{r}{w(\zeta_0)}$ , the intensity profile reads

$$I_{\mathcal{N}}^{\zeta_0}(\zeta = \zeta_0) = 4\sqrt{\frac{2}{\pi}} e^{-2(\frac{z_0-t}{\tau/2})^2} \frac{1}{1+\zeta_0^2} \frac{W}{\pi w_0^2 \tau} \frac{1}{C_{\mathcal{N}}^2} \times \left( \sum_{p=0}^{\mathcal{N}} (-1)^p c_{p,\mathcal{N}} L_p(2\chi^2) \right)^2 e^{-2\chi^2}. \quad (7)$$

For the special case of a FG $_{\mathcal{N}}$  field profile to be implemented in the beam focus at  $\zeta_0 = 0$  we have  $\varphi_p \rightarrow p\pi$  [18, 19], while for a FG $_{\mathcal{N}}$  beam profile in the far field at  $\zeta_0 \gg 1 \leftrightarrow \zeta_0 \rightarrow \infty$ , we have  $\varphi_p \rightarrow 2p\pi$ . This difference can be attributed to the additional factor of  $(-1)^{p'-p}$  in the far field intensity profile not present in the focus; cf. the discussion below Eq. (3). Noteworthy, it implies the following far-field/focus dualities, which hold up to an obvious overall normalization factor: (i) The far-field profile  $I_{\mathcal{N}}^0(\zeta \gg 1)$  of a beam featuring a FG $_{\mathcal{N}}$  focus profile matches the focus profile  $I_{\mathcal{N}}^\infty(\zeta = 0)$  of a beam with a FG $_{\mathcal{N}}$  far-field profile and vice versa. (ii) In the two special cases characterized by either  $\zeta_0 = 0$  or  $\zeta_0 \rightarrow \infty$  the far-field  $I_{\mathcal{N}}^{\zeta_0}(\zeta \gg 1)$  and focus  $I_{\mathcal{N}}^{\zeta_0}(\zeta = 0)$  profiles are related by the substitution  $c_{p,\mathcal{N}} \rightarrow (-1)^p c_{p,\mathcal{N}}$ .

In a next step, we show that the superposition of two laser fields  $E_{\mathcal{N}}^{\zeta_0}(x)$  characterized by the same values of  $w_0$  and  $\tau$  but different  $\mathcal{N}$  and  $W$  allows for the implementation of a laser field exhibiting a field-free hole in its center at  $\zeta = \zeta_0$ . To achieve this, we subtract the two field profiles, i.e., determine  $E_{\mathcal{N},\mathcal{N}'}^{\zeta_0}(x) = E_{\mathcal{N}}^{\zeta_0}(x) - E_{\mathcal{N}'}^{\zeta_0}(x)$  with  $\mathcal{N} > \mathcal{N}'$ , while ensuring that both fields have the same peak field amplitude at  $\zeta_0$ ; the intensity profile of the resulting field is  $I_{\mathcal{N},\mathcal{N}'}^{\zeta_0}(x)$ . The latter condition can be enforced by requiring the energy  $W'$  of the FG $_{\mathcal{N}'}$  beam to fulfill  $W' = (\frac{C_{\mathcal{N}'}}{C_{\mathcal{N}}})^2 W$ . The resulting FG $_{\mathcal{N},\mathcal{N}'}^{\zeta_0}$  field can be expressed in a form very similar to that of a single FG $_{\mathcal{N}}$  field: in order to implement it, the mode-specific phases and energies have to be chosen as in Eq. (5), with the minor modification that now

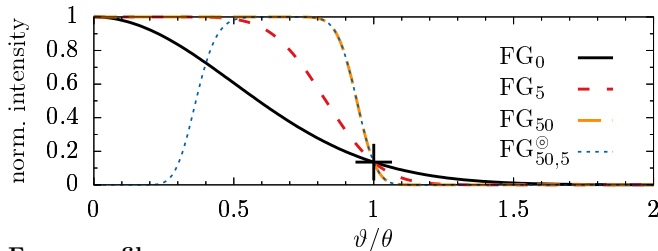
$$c_{p,\mathcal{N}} \rightarrow c_{p,\mathcal{N}} - \Theta(\mathcal{N}' - p) c_{p,\mathcal{N}'}, \quad (8)$$

with Heaviside function  $\Theta(\cdot)$ . The pulse energy  $W_{\mathcal{N},\mathcal{N}'}$  is obtained by summing up the mode energies (5) with Eq. (8). Field-free rings can be implemented along the same lines but require the superposition of more beams.

*Flattened-Gaussian far-field profiles* In the remainder of this letter, we focus on the special case of  $\zeta_0 \gg 1$  and thus only consider laser beams characterized by

FG $_{\mathcal{N}}$  or FG $_{\mathcal{N},\mathcal{N}'}$  far-field profiles. The respective far-field intensity profiles  $I^\infty(\zeta \gg 1)$  follow from Eq. (7) for  $\zeta = \zeta_0 \gg 1$ , implying  $\chi \simeq \frac{\vartheta}{\theta}$  and  $\frac{1}{1+\zeta_0^2} \simeq \frac{1}{\zeta^2}$ . Moreover, the far-field/focus duality (ii) predicts the focus intensity profiles  $I^\infty(\zeta = 0)$  to result from Eq. (7) upon replacing  $\zeta = \zeta_0 = 0$  and  $c_{p,\mathcal{N}} \rightarrow c_{p,\mathcal{N}}(-1)^p$ . For a graphical representation of the far-field and focus profiles of FG $_{\mathcal{N}}$  and FG $_{\mathcal{N},\mathcal{N}'}$  profiles implemented in the far field, see Fig. 1.

#### Far-field transverse intensity profiles:



#### Focus profiles:

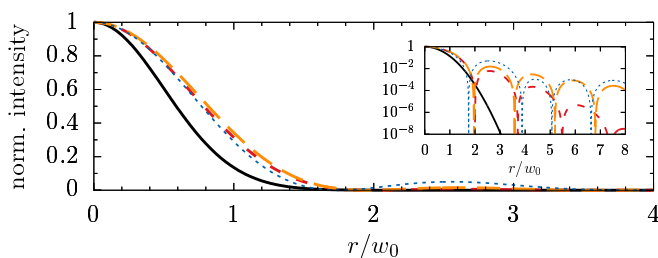


FIG. 1. Upper panel: Far-field intensity profiles  $I^\infty(\zeta \gg 1)$  of FG $_{\mathcal{N}}$  and FG $_{\mathcal{N},\mathcal{N}'}$  beams as a function of  $\vartheta$  measured in units of the asymptotic divergence  $\theta$  of the FG $_0$  beam. Here, the waist parameters  $w_0$  determining the angular spread of the far-field profiles via  $\theta \simeq \frac{\lambda}{\pi w_0}$  are rescaled as  $w_0 \rightarrow r_{\mathcal{N}} w_0$  such that  $\theta_{\mathcal{N}} \rightarrow \theta$ . The cross highlights the matching point. Lower panel: Associated focus profiles  $I^\infty(\zeta = 0)$  as a function of the beam radius measured in units of the FG $_0$  beam waist  $w_0$ ; the inset shows the same curves, adopting a logarithmic scale. Deviations between the curves and the emergence of Airy rings are particularly visible in the logarithmic plot.

To allow for a better comparison of the focus profiles associated with different FG $_{\mathcal{N}}$  far-field profiles, we introduce effective waists  $w_{\mathcal{N}}$ . The latter are defined as the  $1/e^2$  radii of the intensity profiles  $I_{\mathcal{N}}^\infty(x)$  in the focus at  $\zeta = 0$ , resulting in the defining equation

$$\sum_{p=0}^{\mathcal{N}} c_{p,\mathcal{N}} L_p(2s_{\mathcal{N}}^2) = e^{s_{\mathcal{N}}^2 - 1} \sum_{p=0}^{\mathcal{N}} c_{p,\mathcal{N}}, \quad (9)$$

where the scaling parameter  $s_{\mathcal{N}} = \frac{w_{\mathcal{N}}}{w_0}$  measures  $w_{\mathcal{N}}$  in units of  $w_0$ . Equation (9) can be straightforwardly solved numerically for  $w_{\mathcal{N}}$ . Generically, the larger  $\mathcal{N}$ , the wider the FG $_{\mathcal{N}}$  radial field profile for fixed  $w_0$  [18, 19]. For the present scenario, where the FG $_{\mathcal{N}}$  profile is implemented in the far field, this implies that the larger  $\mathcal{N}$ , the smaller the effective beam divergence. This translates into  $w_{\mathcal{N}+1} < w_{\mathcal{N}}$ , and thus implies  $s_{\mathcal{N}} < 1$  for

$\mathcal{N} \geq 1$ . Resorting to an expansion in  $s_{\mathcal{N}} < 1$  of Eq. (9) up to quadratic order, for  $\mathcal{N} \geq 1$  we obtain the estimate

$$s_{\mathcal{N}}^2 \approx \frac{(1 - e^{-1}) \sum_{p=0}^{\mathcal{N}} c_{p,\mathcal{N}}}{\sum_{p=0}^{\mathcal{N}} (2p + e^{-1}) c_{p,\mathcal{N}}}. \quad (10)$$

Similarly, the peak intensity in the focus can be related as  $I_{\mathcal{N}}^\infty(r = z = 0) = \sigma_{\mathcal{N}} I_0(0, t)$  to the focus peak intensity of the FG $_0$  beam; its on-axis intensity profile is  $I_0(z, t) = 4\sqrt{\frac{2}{\pi}} e^{-2(\frac{z-t}{\tau})^2} \frac{1}{1+\zeta^2} \frac{W}{\pi w_0^2 \tau}$ . This scaling factor is given by

$$\sigma_{\mathcal{N}} = \frac{1}{C_{\mathcal{N}}^2} \left( \sum_{p=0}^{\mathcal{N}} c_{p,\mathcal{N}} \right)^2. \quad (11)$$

Upon insertion of Eq. (6), the sums in Eqs. (10) and (11) can be performed, yielding  $s_{\mathcal{N}}^2 \approx \frac{2(1-e^{-1})}{\mathcal{N}+2e^{-1}}$  and  $\sigma_{\mathcal{N}} = \frac{(\mathcal{N}+1)^2}{C_{\mathcal{N}}^2}$ . With Eq. (8) we moreover find  $s_{\mathcal{N},\mathcal{N}'}^2 \approx \frac{2(1-e^{-1})}{\mathcal{N}+\mathcal{N}'+1+2e^{-1}}$  and  $\sigma_{\mathcal{N},\mathcal{N}'} = \frac{(\mathcal{N}-\mathcal{N}')^2}{C_{\mathcal{N}}^2}$ , characterizing the effective waist  $w_{\mathcal{N},\mathcal{N}'} = s_{\mathcal{N},\mathcal{N}'} w_0$  and focus peak intensity  $I_{\mathcal{N},\mathcal{N}'}^\infty(r = z = 0) = \sigma_{\mathcal{N},\mathcal{N}'} I_0(0, t)$  of an FG $_{\mathcal{N},\mathcal{N}'}$  beam. As the two FG $_{\mathcal{N}}$  beams superimposed to form the latter fulfill  $\mathcal{N} > \mathcal{N}'$  and  $w_{\mathcal{N}} \leq w_0$ , we have  $s_{\mathcal{N},\mathcal{N}'} < 1$ .

Analogously, effective asymptotic divergences  $\theta_{\mathcal{N}}$  can be defined for the FG $_{\mathcal{N}}$  beams as the polar angle for which the far-field intensity drops by a factor of  $1/e^2$  relatively to its on-axis peak value. These follow from Eq. (9) upon substitution of  $c_{p,\mathcal{N}} \rightarrow (-1)^p c_{p,\mathcal{N}}$  and  $s_{\mathcal{N}} \rightarrow r_{\mathcal{N}} = \frac{\theta_{\mathcal{N}}}{\theta}$ , resulting in the condition  $\sum_{n=0}^{\mathcal{N}} \frac{1}{n!} r_{\mathcal{N}}^{2n} = e^{r_{\mathcal{N}}^2 - 1}$ . While the zeros of this equation can be readily determined numerically, it is approximately solved by  $r_{\mathcal{N}} \approx \sqrt{1 + \mathcal{N}}$ . The scaling factor of the peak intensity in the far field  $I_{\mathcal{N}}^\infty(\zeta \gg 1) = \rho_{\mathcal{N}} I_0(z \gg z_R, t)$  again follows from the focus result (11) upon substitution of  $c_{p,\mathcal{N}} \rightarrow (-1)^p c_{p,\mathcal{N}}$ , implying  $\rho_{\mathcal{N}} = 1/C_{\mathcal{N}}^2$ . The inner and outer asymptotic divergences of an FG $_{\mathcal{N},\mathcal{N}'}$  beam are determined by  $\theta_{\mathcal{N}}$  and  $\theta_{\mathcal{N}'}$ . Moreover, by construction the far-field peak intensity of such a beam equals  $I_{\mathcal{N}}^\infty(\zeta \gg 1)$ .

Finally, we note that taking into account the large- $\mathcal{N}$  scaling of  $C_{\mathcal{N}}^2 \sim \mathcal{N}$  [19], for large values of  $\mathcal{N}$  we have  $\sigma_{\mathcal{N}} s_{\mathcal{N}}^2 \sim \rho_{\mathcal{N}} r_{\mathcal{N}}^2 \sim \text{const}$ . This is consistent, as the  $\mathcal{N}$  independent laser pulse energy should be proportional to the product of peak intensity and beam radius squared.

*Exemplary results* Subsequently we demonstrate the novel possibilities enabled by the use of beams featuring a peak in the focus but a hole in the far field for nonlinear QED experiments on the example of vacuum birefringence [21]: linearly polarized probe photons traversing a strong pump field can pick up an ellipticity if their polarization vector has a non-vanishing overlap with the two distinct polarization eigenmodes imprinted on the quantum vacuum by the pump field. This results in polarization-flipped signal photons constituting the experimental signature of the effect. The head-on collision of an XFEL probe and a high-intensity pump constitutes

a promising route to its first measurement [22–31]. Recently, it has been shown that employing the scattering of signal photons outside the forward-cone of the probe notably enhances the perspectives of measuring the effect for given parameters [27, 29, 30]. Replicating this scenario with probe beams featuring a hole in the far-field seems particularly promising: it should facilitate an essentially background-free measurement of the signal photons scattered in the direction of the forward beam axis.

All-optical quantum vacuum signatures are efficiently studied in the vacuum emission picture [32, 33]. In this approach, photonic signals of quantum vacuum nonlinearities in macroscopic electromagnetic fields are encoded in signal photons emitted from the strong-field region where the driving fields overlap. The results presented below are based on the leading term of the Heisenberg-Euler Lagrangian [1, 2, 34]. For electric  $E$  (magnetic  $B$ ) fields much smaller than the critical field  $E_{\text{cr}} = \frac{m_e^2}{e} \simeq 1.3 \times 10^{18} \frac{\text{V}}{\text{m}}$  ( $B_{\text{cr}} \simeq 4.4 \times 10^9 \text{ T}$ ), varying on spatial scales much larger than the Compton wavelength  $\lambda_{\text{C}} = \frac{1}{m_e} \simeq 3.9 \times 10^{-13} \text{ m}$ , this should allow for the accurate theoretical study of all-optical QED vacuum phenomena. These conditions are perfectly fulfilled by state-of-the-art XFEL and high-intensity laser fields.

Here, we consider the head-on collision of an  $\text{LG}_{p,0}$  x-ray pulse (1) propagating in positive  $z$  direction with a  $\text{FG}_0$  high-intensity laser pulse (energy  $\tilde{W}$ , duration  $\tilde{\tau}$ , waist  $\tilde{w}_0$  and Rayleigh range  $\tilde{z}_R$ ;  $\tilde{w}(z) = \tilde{w}_0 \sqrt{1 + (\frac{z}{\tilde{z}_R})^2}$ ) at zero impact parameter. Both pulses are linearly polarized and the angle between their polarization vectors is  $\frac{\pi}{4}$  rad, such that the number of signal photons scattered in a  $\perp$ -polarized mode is maximized. As x-rays fulfill  $\zeta \ll 1$  throughout the interaction region, we can adopt the approximation  $\zeta \approx 0$  and thus  $w(z) \approx w_0$  when determining the vacuum emission amplitude [29]. The intensity profile of the high-intensity pulse follows from Eq. (3) upon limitation to  $p = p' = 0$ , substitution of  $z \rightarrow -z$  and transition to tilded quantities.

Apart from the choice of the laser field profiles, this scenario matches the one detailed in Sec. 4.2 of Ref. [11]: the differential number of  $\perp$ -polarized signal photons of x-ray frequency amounts to the  $+$  component of Eq. (44) with  $p \rightarrow \perp$ , while neglecting the manifestly inelastic terms in Eq. (41) is equivalent to replacing the square of the pump field with its intensity profile; cf. also Eq. (11) of [29]. Hence, the differential number of  $\perp$ -polarization x-ray photons of energy  $k = |\vec{k}|$  reads

$$d^3 N_{\perp} \simeq \frac{d^3 k}{(2\pi)^3} \frac{32}{225} \alpha^4 \frac{k}{m_e^8} \left| \sum_p \mathcal{M}_p \right|^2, \quad (12)$$

with

$$\mathcal{M}_p = \int d^4 x e^{i(\vec{k}\vec{x} - kt)} \mathcal{E}_p(x) \Big|_{\zeta \ll 1} \tilde{I}(x). \quad (13)$$

All Fourier integrals apart from the one over the longitudinal coordinate  $z$  can be performed analytically. Accounting only for the dominant quasielastic contributions [27, 29], Eq. (13) can be expressed compactly as

$$\begin{aligned} \mathcal{M}_p \simeq & \left( \frac{8}{\pi} \right)^{\frac{3}{4}} \frac{\tilde{W} \sqrt{\tilde{\tau}}}{w_0 T_{\pm}} e^{-\left(\frac{\tilde{\tau}\tilde{\tau}}{4T_{\pm}}\right)^2 (k-\omega)^2} \sqrt{\tilde{W}_p} e^{-i\varphi_p} \\ & \times \int_{-\infty}^{\infty} dz \frac{[2 - r^2(z)]^p}{[2 + r^2(z)]^{p+1}} L_p \left( \frac{k_{\perp}^2 \tilde{w}^2(z) r^2(z)}{2[r^4(z) - 4]} \right) \\ & \times e^{-\frac{k_{\perp}^2 \tilde{w}^2(z)}{4[2+r^2(z)]} - 2\left(\frac{4z}{T_{\pm}}\right)^2} e^{i[(k-\omega)\left(\frac{T_{\pm}}{T_{\pm}}\right)^2 + k_z - \omega]z}, \quad (14) \end{aligned}$$

where  $k_{\perp}^2 = k_x^2 + k_y^2$ ,  $T_{\pm} = \sqrt{2\tau^2 \pm \tilde{\tau}^2}$  and  $r(z) = \frac{\tilde{w}(z)}{w_0}$ . In the derivation of Eq. (14) we made use of  $L_p(2\chi^2)e^{-\chi^2} = L_p(-2\partial_b)e^{-b\chi^2} \Big|_{b=1}$  and resorted to the identity  $L_p(-2\partial_b) \frac{1}{2+bc} e^{-\frac{a}{2+bc}} \Big|_{b=1} = e^{-\frac{a}{2+c}} \frac{[2-c]^p}{[2+c]^{p+1}} L_p\left(\frac{2ac}{c^2-4}\right)$  which follows from standard algebraic operations and [35]. Subsequently we use spherical coordinates  $k_z = k \cos \vartheta$ ,  $k_{\perp}^2 = k^2 \sin^2 \vartheta$  and  $d^3 k = k^2 dk d\cos \vartheta d\varphi$ , and study the birefringence phenomenon with an  $\text{FG}_{\mathcal{N},\mathcal{N}'}$  probe beam. To this end we substitute Eq. (5) with coefficients (8) into Eq. (14). As an example we choose  $\mathcal{N} = 50$  and  $\mathcal{N}' = 5$ ; see Fig. 2.

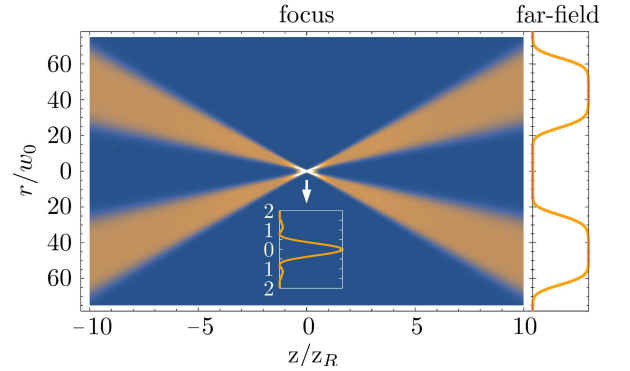


FIG. 2. Laser intensity  $I_{50,5}^{\infty}(x)$  as function of the longitudinal coordinate  $z$  measured in units of the Rayleigh range  $z_R$ , and the radial distance  $r$  measured in units of the waist  $w_0$  of the  $\text{FG}_0$  mode. The color scale is such that the higher the intensity, the brighter the color: the intensity vanishes in the dark regions and reaches its maximum in the beam focus at  $z = r = 0$ . The inset shows the transverse focus profile; on the right we depict the far-field intensity profile.

The original XFEL probe is assumed to feature a  $\text{FG}_{50}$  far-field profile and deliver pulses of duration  $\tau = 25$  fs encompassing  $N_0 = 10^{12}$  photons of energy  $\omega = 12914 \text{ eV}$ ; the pulse energy is  $W = N_0 \omega$ . The polarization of x-ray photons of this energy can be measured with a purity of  $\mathcal{P} = 5.7 \times 10^{-10}$  [36]. We envision the  $\text{FG}_{50,5}^{\circ}$  profile to be obtained therefrom by adequately blocking the x-ray photons at small  $\vartheta$ , thereby reducing the number  $N$  of photons in the  $\text{FG}_{50,5}^{\circ}$  pulse; cf. Fig. 1 (upper panel). For the high-intensity laser we adopt the parameters of the high-intensity laser installed at the Helmholtz International

Beamline for Extreme Fields (HIBEF) [37] at the European XFEL [38]. It delivers pulses of energy  $\tilde{W} = 10$  J and duration  $\tilde{\tau} = 25$  fs at a wavelength of  $\lambda = 800$  nm and a repetition rate of 5 Hz. The high-intensity laser is assumed to be focused to a waist of  $\tilde{w}_0 = 1$   $\mu\text{m}$ . For the  $\text{FG}_{50,5}^{\circledast}$  probe we choose  $w_0 = 3.3$   $\mu\text{m}$ , such that  $w_{50,5} \simeq 0.55$   $\mu\text{m}$ . For these parameters, Eq. (12) predicts  $N_{\perp} \simeq 1.47$   $\perp$ -polarized signal photons per shot, to be compared with the total number of x-ray photons available for probing  $N \simeq 8.63 \times 10^{11}$ ;  $N_0 - N \simeq 1.37 \times 10^{11}$  photons otherwise filling the hole are blocked. Figure 3 shows that  $\frac{dN}{\vartheta d\vartheta}$  reaches its maximum in a plateau at small values of  $\vartheta \lesssim 20$   $\mu\text{rad}$  and slowly decays towards larger values of  $\vartheta$ . In the same angular interval, the photon distribution of the probe pulse exhibits a hole, suggesting the possibility of an efficient signal-to-background separation.

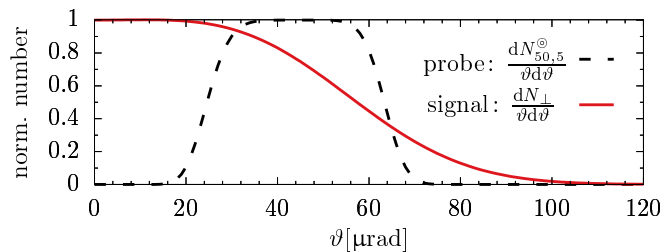


FIG. 3. Far-field angular decay of the probe photons and the polarization-flipped signal photons for the parameters detailed in the main text. This figure highlights the potential of  $\text{FG}_{N,N'}^{\circledast}$  laser beams in achieving an essentially background-free measurement of the signal at both small and large  $\vartheta$ , where the differential number of probe photons traversing the interaction region unaffected decays faster than the signal.

Reducing  $w_0$  for fixed  $\tilde{w}_0$ , the plateau disappears and the signal also starts to diminish towards small  $\vartheta$ , resulting in a peak at finite  $\vartheta$ . Conversely, when increasing  $w_0$  the plateau becomes narrower, eventually resulting in a narrow peak at  $\vartheta = 0$ . Besides, the signal drops as less probe photons traverse the strong field region. In turn, both variations tend to reduce the attainable signal.

Accounting for the finite purity of polarization filtering, only signal photons fulfilling  $\frac{dN_{\perp}}{\vartheta d\vartheta} \geq \mathcal{P} \frac{dN}{\vartheta d\vartheta}$  can be measured above the background of the XFEL photons traversing the strong field region unaffected. This criterion is met for  $0 \leq \vartheta \leq 15$   $\mu\text{rad}$  and  $\vartheta \geq 76$   $\mu\text{rad}$ . The numbers of discernible signal photons per shot are  $N_{\perp}^{\text{dis.}}|_{\vartheta \leq 15 \mu\text{rad}} \simeq 0.094$  and  $N_{\perp}^{\text{dis.}}|_{\vartheta \geq 76 \mu\text{rad}} \simeq 0.14$ . While the former are emitted into a solid angle of  $\approx 700$   $\mu\text{rad}^2$ , the emission angle for the latter is  $\approx 30$  times larger. The first signal is particularly promising. Its measurement only requires a detector with small angular acceptance and no recollimation is needed for an efficient detection.

*Conclusions and Outlook* Our findings underpin the potential of beams featuring a peak in the focus, but a hole in the far field for strong-field QED experiments.

Certainly, many other signatures of quantum vacuum nonlinearity can be critically enhanced by such tailored beams. This is especially true for scenarios based on the collision of high-intensity laser pulses, usually characterized by a paradox: while most signal photons arise from quasielastic scattering processes, for standard beams their measurement is typically obstructed by the background of the driving laser photons. Thus, though containing much less photons, inelastic channels constitute the most prospective experimental signatures [39]. The use of tailored beams can change this and make quasielastically scattered signals experimentally accessible.

This work has been funded by the Deutsche Forschungsgemeinschaft (DFG) under Grant No. 416607684 within the Research Unit FOR2783/1 and was supported by the German Academic Exchange Service (DAAD) under the ‘‘Mikhail Lomonosov’’ Programme. Moreover, E.A.M. would like to thank the Helmholtz Institute Jena for hospitality and support. We are grateful to Matt Zepf for helpful discussions, and to Holger Gies for valuable comments on the manuscript.

\* felix.karbstein@uni-jena.de

† mosmanea@tpu.ru

- [1] H. Euler and B. Kockel, *Naturwiss.* **23**, no. 15, 246 (1935).
- [2] W. Heisenberg and H. Euler, *Z. Phys.* **98**, no. 11-12, 714 (1936), an English translation is available at [physics/0605038].
- [3] E. S. Fradkin, D. M. Gitman and S. M. Shvartsman, Berlin, Germany: Springer (1991) 288 p. (Springer series in nuclear and particle physics)
- [4] W. Dittrich and H. Gies, *Springer Tracts Mod. Phys.* **166**, 1 (2000).
- [5] M. Marklund and P. K. Shukla, *Rev. Mod. Phys.* **78**, 591 (2006) [hep-ph/0602123].
- [6] A. Di Piazza, C. Müller, K. Z. Hatsagortsyan and C. H. Keitel, *Rev. Mod. Phys.* **84**, 1177 (2012) [arXiv:1111.3886 [hep-ph]].
- [7] G. V. Dunne, *Int. J. Mod. Phys. A* **27**, 1260004 (2012) [arXiv:1202.1557 [hep-th]].
- [8] R. Battesti and C. Rizzo, *Rept. Prog. Phys.* **76**, no. 1, 016401 (2013) [arXiv:1211.1933 [physics.optics]].
- [9] B. King and T. Heinzl, *High Power Laser Science and Engineering*, 4, e5 (2016) [arXiv:1510.08456 [hep-ph]].
- [10] T. Inada, T. Yamazaki, T. Yamaji, Y. Seino, X. Fan, S. Kamioka, T. Namba and S. Asai, *Applied Sciences* **7**, 671 (2017) [arXiv:1707.00253 [hep-ex]].
- [11] F. Karbstein, *Particles* **3**, no. 1, 39 (2020) [arXiv:1912.11698 [hep-ph]].
- [12] CILEX, <http://cilexsaclay.fr>.
- [13] CoReLS, <http://corels.ibs.re.kr>.
- [14] ELI, <https://eli-laser.eu>.
- [15] X. Xie, J. Zhu, Q. Yang, J. Kang, H. Zhu, M. Sun and A. Guo, *CLEO Technical Digest*, paper SM1M.7 (2016).
- [16] A. E. Siegman, *Lasers*, 1st ed., University Science Books, Herndon, USA (1986).
- [17] B. E. A. Saleh and M. C. Teich, *Fundamentals of Photonics*, 1st ed., John Wiley & Sons, New York, USA (1991).
- [18] F. Karbstein and E. A. Mosman, *Phys. Rev. D* **96**, no.

- 11, 116004 (2017) [arXiv:1711.06151 [hep-ph]].
- [19] F. Gori, Optics Communications **107**, 335-341 (1994).
- [20] C. Palma and V. Bagini, Optics Communications **111**, 6-10 (1994).
- [21] J. S. Toll, Ph.D. thesis, Princeton Univ., 1952 (unpublished).
- [22] E. B. Aleksandrov, A. A. Ansel'm, A. N. Moskalev, Zh. Eksp. Teor. Fiz. **89**, 1181 (1985) [Sov. Phys. JETP **62**, 680 (1985)].
- [23] T. Heinzl, B. Liesfeld, K. U. Amthor, H. Schwöerer, R. Sauerbrey and A. Wipf, Opt. Commun. **267**, 318 (2006) [hep-ph/0601076].
- [24] A. Di Piazza, K. Z. Hatsagortsyan and C. H. Keitel, Phys. Rev. Lett. **97**, 083603 (2006) [hep-ph/0602039].
- [25] V. Dinu, T. Heinzl, A. Ilderton, M. Marklund and G. Torgrimsson, Phys. Rev. D **89**, no. 12, 125003 (2014) [arXiv:1312.6419 [hep-ph]].
- [26] V. Dinu, T. Heinzl, A. Ilderton, M. Marklund and G. Torgrimsson, Phys. Rev. D **90**, no. 4, 045025 (2014) [arXiv:1405.7291 [hep-ph]].
- [27] F. Karbstein, H. Gies, M. Reuter and M. Zepf, Phys. Rev. D **92**, no. 7, 071301 (2015) [arXiv:1507.01084 [hep-ph]].
- [28] H. -P. Schlenvoigt, T. Heinzl, U. Schramm, T. Cowan and R. Sauerbrey, Physica Scripta **91**, 023010 (2016).
- [29] F. Karbstein and C. Sundqvist, Phys. Rev. D **94**, no. 1, 013004 (2016) [arXiv:1605.09294 [hep-ph]].
- [30] F. Karbstein, Phys. Rev. D **98**, no. 5, 056010 (2018) [arXiv:1807.03302 [quant-ph]].
- [31] F. Karbstein and E. A. Mosman, Phys. Rev. D **100**, no. 3, 033002 (2019) [arXiv:1906.10122 [physics.optics]].
- [32] D. Galtsov and V. Skobelev, Phys. Lett. B **36**, 238 (1971).
- [33] F. Karbstein and R. Shaisultanov, Phys. Rev. D **91**, no. 11, 113002 (2015) [arXiv:1412.6050 [hep-ph]].
- [34] J. S. Schwinger, Phys. Rev. **82**, 664 (1951).
- [35] <http://functions.wolfram.com/05.02.23.0003.01> .
- [36] B. Marx *et al.*, Phys. Rev. Lett. **110**, no. 25, 254801 (2013).
- [37] HIBEF, <https://hibef.eu> .
- [38] XFEL, <https://xfel.eu> .
- [39] F. Karbstein, A. Blinne, H. Gies and M. Zepf, Phys. Rev. Lett. **123**, no. 9, 091802 (2019) [arXiv:1905.00858 [hep-ph]].